Journal of Radiation Research, Vol. 64, No. 6, 2023, pp. 973–981
https://doi.org/10.1093/jrr/rrad075
Advance Access Publication: 15 October 2023

Evaluations of patient-specific bolus fabricated by mold-and-cast method using computer numerical control machine tools†

Geum Bong Yu[1,2], Jimin Kwon[1,3], Seunghoon Chae[1], Sung Young Lee[1] and Seongmoon Jung[1,2,4,5,*]

[1]Department of Radiation Oncology, Seoul National University Hospital, Seoul 03080, Republic of Korea
[2]Institute of Radiation Medicine, Seoul National University Medical Research Center, Seoul 03080, Republic of Korea
[3]Department of Mechanical and Industrial Engineering, University of Toronto, Toronto M5S 3G8, Ontario, Canada
[4]Biomedical Research Institute, Seoul National University Hospital, Seoul 03080, Republic of Korea
[5]Department of Nuclear Engineering, Ulsan National Institute of Science and Technology, Ulsan 44919, Republic of Korea
*Corresponding author. Department of Radiation Oncology, Seoul National University Hospital, 101, Daehak-ro, Jongno-gu, Seoul 03080, Republic of Korea. Tel: +82-2-20-72-41-60; Fax: +82-2-6072-5167; Email: smjung@snu.ac.kr

†Presentation at a conference: Oral presentation at the Korean Association for Radiation Protection spring meeting, 26–28 April, Busan, South Korea.
(Received 20 December 2022; revised 19 January 2023; editorial decision 24 March 2023)

ABSTRACT

The patient-specific bolus fabricated by a mold-and-cast method using a 3D printer (3DP) and silicon rubber has been adopted in clinical practices. Manufacturing a mold using 3DP, however, can cause time delays due to failures during the 3D printing process. Thereby, we investigated an alternative method of the mold fabrication using computer numerical control (CNC) machine tools. Treatment plans were conducted concerning a keloid scar formed on the ear and nose. The bolus structures were determined in a treatment planning system (TPS), and the molds were fabricated using the same structure file but with 3DP and CNC independently. Boluses were then manufactured using each mold with silicone rubbers. We compared the geometrical difference between the boluses and the planned structure using computed tomography (CT) images of the boluses. In addition, dosimetric differences between the two measurements using each bolus and the differences between the measured and calculated dose from TPS were evaluated using an anthropomorphic head phantom. Geometrically, the CT images of the boluses fabricated by the 3DP mold and the CNC mold showed differences compared to the planned structure within 2.6 mm of Hausdorff distance. The relative dose difference between the measurements using either bolus was within 2.3%. In conclusion, the bolus made by the CNC mold benefits from a stable fabricating process, retaining the performance of the bolus made by the 3DP mold.

Keywords: patient-specific bolus; computer numerical control tools; electron conformal radiation therapy; keloid treatment

INTRODUCTION

Flat sheets of commercial bolus have been widely used to deliver prescribed dose to surface lesion during radiation therapy. The bolus performs as a skin-equivalent material, thus compensating for lacking build-up depth in the treatment. However, irregular surfaces, such as ear, nose, hand, foot and scalp, have an intrinsic limitation resulting in generating unwanted air gaps between the skin and the bolus [1–4]. Many studies propose fabrication of a patient-specific 3D bolus (denoted as a 3D bolus) as the solution to reduce the air gap [5–8]. In the early stages of producing the 3D bolus, it was fabricated directly out of a 3D printer (3DP) using classic printable thermoplastic filaments: namely, acrylonitrile butadiene styrene and polylactic acid [9, 10]. However, the early 3D-printed boluses gave rise to fitting issues due to their structural rigidity, thus producing an unexpected air gap. Consequently, the selection of flexible materials became a focal point of the 3D bolus production. Changing the material naturally modified the fabrication method: from directly printing bolus to printing a 3D mold and casting flexible material into the mold [11–13]. Continued study and actual treatment cases steadily enhanced the mold-and-cast fabrication method involving 3DP.

Despite the enhancements, the involvement of the 3DP in the fabrication process inherits several limitations. Printing complex structures requires postprocessing after completion of the printing [14–16], which decreases a work efficiency and increases the labor intensity. The 3D printing process is sensitive to environmental temperature and humidity. When the 3DP is operated in an unwanted environment, warping and deformation can occur in the mold-printing process, directly affecting quality of the printed mold and thus the structure of the casted 3D bolus. Other than the environmental issues, 3D printing is susceptible to many other issues, such as nozzle clogging, overhang, etc., that must be avoided by an iterative loop process of test printing followed by adjustment of the settings. Overall, to achieve a highly accurate 3D printed structure, the user must optimize environmental setups and printer settings through an iterative test printing until it no more fails. This iterative process for accurate fabrication unavoidably costs time and material.

Therefore, an alternative method of mold fabrication, using a computer numerical control (CNC) machine tool, which refers to an automated tool controlled by a computer, has a potential of avoiding labor-intensive work, time delay, and inefficiency. The machining refers to a subtractive manufacturing, i.e. cutting away the material, while the material is stacked, thus representing an additional manufacturing in the 3D printing. The CNC machine was used to fabricate the 3D bolus itself exploiting a resin-impregnated wax having a physical density of 0.92 g/cm^3 [17], which had a rigid structure and was not a tissue-equivalent material. In this study, we propose the CNC as an alternative to the 3DP in the fabrication process of the 3D bolus mold. The boluses fabricated by the CNC and 3DP (in a conventional way) were geometrically evaluated by a comparison between computed tomography (CT) images of the boluses and the planned structured sets in terms of Hausdorff distance [18, 19]. In addition, dose measurements were performed using the metal oxide semiconductor field effect transistor (MOSFET) detector to compare the dosimetric differences between the boluses fabricated by the CNC and the 3DP.

MATERIALS AND METHODS

Treatment setup

To evaluate the performance of the 3D bolus, keloid scars on the curvy parts of the body, the tubercle of the ear and the ala of the nose, were considered. A keloid scar is a benign growth of dense fibrous tissue arising from an abnormal healing response to an injury, extending beyond the original borders of the wound. Even after a surgical excision, a recurrence rate of the keloid scar is ∼45–100% [20]. The rate reduces to under 20% if the keloid scar is treated with radiation within 72 h after the excision [21–27].

For the dosimetric evaluation of the boluses we applied 10 Gy electron beam irradiation in a single fraction, following the radiotherapy protocol for the keloid treatment [28]. A PH-76 Dental Radiography Head Phantom (model 41 301–400, KYOTO KANJUKU CO. LTD, Kyoto, Japan) was used for a treatment plan and delivery. The treatment lesions were shown in laser crossings on the phantom in Fig. 1. Around the targeted keloid lesion, two points, marked by A and B, were selected for the measurement of the delivered dose.

CT scans of the head phantom were performed using Brilliance CT Big Bore™ (Royal Philips Electronics, Amsterdam, the Netherlands).

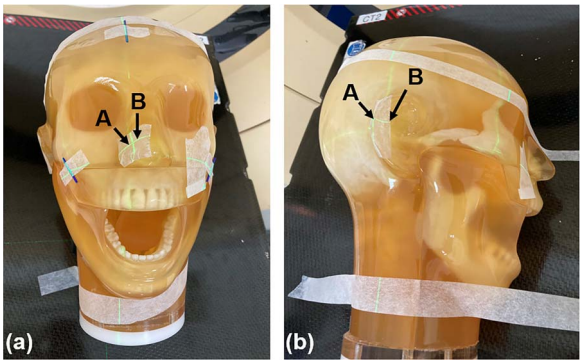

Fig. 1. Head phantom with assumed treatment lesions marked with room laser crossing on the (a) ala of nose and (b) tubercle of the ear. Two points (A and B) were selected to measure the delivered dose for evaluation.

Table 1. Scan parameters used for the CT (Brilliance CT Big Bore™, Royal Philips Electronics, Amsterdam, the Netherlands)

Scan parameter	Brilliance CT Big Bore™
Field of view	700 mm diameter
Number of pixels	512 × 512
Pixel size	1.3672 × 1.3672 mm^2
Slice thickness	1 mm
Tube voltage	120 kVp

Details of the CT acquisition condition are summarized in Table 1. Reconstructed CT images were sent to the treatment planning system (TPS), Eclipse (v16.1, Varian Medical Systems, Palo Alto, CA, USA). Once the body structure was delineated, the bolus was designed concerning the treatment beam direction and expected dose distribution. For an easier setup and better dose distribution covering the lesion, the top surface of the bolus was designed to be flat and square, and orthogonal to the beam direction. The minimum depth of the tip of the lesion to the surface of the bolus was set to be around 1 cm. For the treatment setup of the bolus and phantom at the isocenter, the laser pathway was marked as a small stud on each side of the bolus top. Due to technical limitations of the current CNC machine setup in our institute, the maximum length of the bolus was constrained to be <6 cm. The bolus design was exported in a DICOM file and then extracted to a stereolithography (STL) file format for the mold fabrication.

The treatment plans were conducted with a 12 MeV electron beam to the ala of the nose as shown in Fig. 2, and a 9 MeV electron beam to the tubercle of the ear as depicted in Fig. 3. For the dose calculation, the electron Monte Carlo (eMC) model (v16.1 in Eclipse) was used with 2% of statistical uncertainty and 2.5 mm of the calculation grid size, but without smoothing. If it were a real treatment case, an additional compensator would have been applied for the extra protection of the normal tissue. However, the current plan was enough to evaluate the delivered dose at selected points near the virtual lesion.

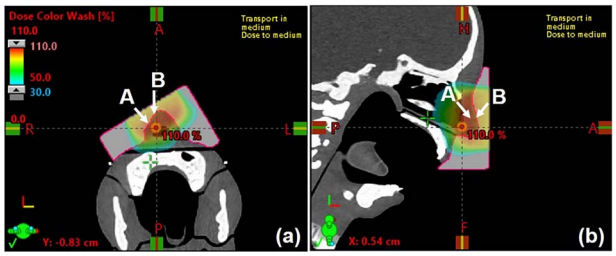

Fig. 2. Treatment plan for the virtual keloid lesion on ala of the nose and expected dose distribution with bolus in transversal (a) and sagittal (b) plane using Eclipse (v16.1, Varian Medical Systems, Palo Alto, CA, USA). Irradiated doses were compared with the calculated doses at point A and B.

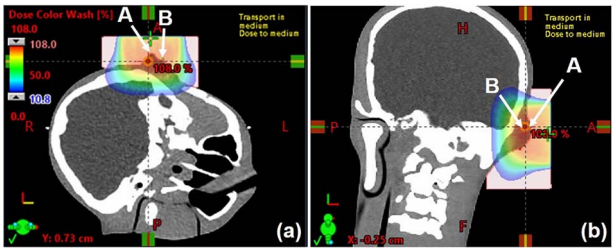

Fig. 3. Treatment plan for the virtual keloid lesion on tubercle of the ear and expected dose distribution with bolus in transversal (a) and sagittal (b) plane using Eclipse (v16.1, Varian Medical Systems, Palo Alto, CA, USA). Irradiated doses were compared with the calculated doses at point A and B.

Preparing the bolus structure

The rough structure of the bolus was retrieved from the radiation treatment structure file (denoted as RS file) to the STL file format. These structures were often not directly manufacturable due to the inevitable slicing between the CT images, which produces cracks and sharp edges within the bolus structure. These file errors in the STL prohibit the structure from being interpreted as a solid body, thereby can result in manufacturing failures. With the Meshmixer, which is a software that allows easy manipulation of mesh files developed by Autodesk (Autodesk, Inc., San Francisco, CA, USA), the rough structures in STL files were processed; first cleaning up unnecessary residue, and then smoothing the rough edges while preserving the shape.

Instruments

Zortrax M300 Dual 3DP (Zortrax S.A., Olsztyn, Poland) and Snapmaker 2.0 CNC (Snapmaker, Shenzhen, Guangdong, China) were used to compare and contrast the two fabrication processes of the 3D bolus. Zortrax has a nozzle diameter of 0.4 mm and a minimum layer thickness of 0.15 mm. Snapmaker CNC can be operated with 0.01 mm increments but to better compare the processes, the minimum vertical axis step-down was limited to 0.15 mm, matching that of Zortrax. Further detailed specifications can be found in Table 2.

Z-HIPS filament is the most frequently used and thus known to cause malfunction the least in the 3D printing. The materials that Snapmaker CNC can cut are wood, acrylic and thin metal. Concerning cost and ease of access, wood stock for sculpting was selected for fabricating the mold.

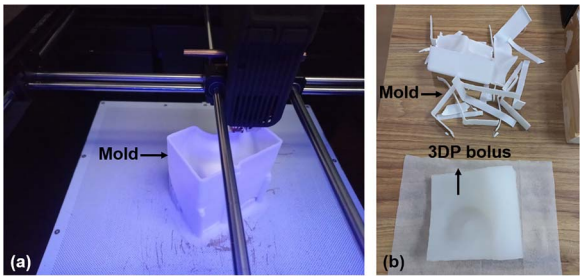

Fig. 4. Molds fabricated by 3DP (a) and their resulting boluses using 3DP mold (b).

3DP molding

We used the fused deposition modeling type of 3DP, where the material was extruded through a nozzle that moves in a computed path to stack layers of materials to form a 3D structure [29, 30]. This was the most cost-effective alternative. Its manufacturing time was greatly dependent on the amount of material used to construct the final print. The mold structure must have a minimum thickness to reduce material usage and thereby printing time, but thick enough to limit leakage of the material. Optimal thickness of the mold was determined to be 1.2 mm through a number of trials of fabricating bolus for clinical usage [9, 11, 12]. Meshmixer was used to generate the shell mold structure by adding a thickness of 1.2 mm to the bolus mesh structure through the 'offset' feature. This shell mold structure was then exported to the 3D printing slicer, which maps horizontal motion of the extruder to print 3D structure layer by layer, in STL file format. Z-suite (v2.6) is the slicer software that generates a 3D printable file compatible with the aforementioned Zortrax printer. The printer settings were set to maximize the accuracy of the final product, with a layer height of 0.15 mm, the maximum accuracy that Zortrax M300 Dual supports. The rest of the printer settings were kept to default at the first trial, which was altered per earlier mentioned printing issues. The manufacturing time for the shell molds took a total of 24 h and 26 h for each ear and nose bolus, including the postprocessing of the print. Pictures of the mold fabricating process and their resulting molds by 3DP are shown in Fig. 4.

CNC molding

CNC is a type of subtractive manufacturing, where the product is created into a shape by removing material away from the initial stock of the material. Its manufacturing time is greatly dependent on the amount of material to be removed and the toolpath that removes the material. The amount of material removal cannot be altered since it is equal to the mold cavity, generated by the bolus structure. The only method to reduce its manufacturing time is to optimize the toolpath. The stock of material was first modeled through computer-aided design software, SOLIDWORKS 2020 (Dassault Systemès SolidWorks Corporation, Waltham, MA, USA). Two mold stocks and the bolus structure were assembled to create the mold cavity using the 'cavity' feature. Two mold cavity structures were then exported to Fusion 3 602 020, a computer-aided manufacturing software developed by

Table 2. Specifications of the molding devices: 3DP (Zortrax S.A., Olsztyn, Poland) and CNC (Snapmaker, Shenzhen, Guangdong, China)

Specifications	Zortrax M300 Dual	Snapmaker 2.0 A350 CNC
Build volume	265 ×265 × 300 mm^3	320 ×350 ×275 mm^3
Tool details	Nozzle diameter 0.4 mm	Spindle Speed 6000–12 000 RPM Shank Diameter 0.5–6.35 mm
Vertical resolution	Layer resolution 0.15–0.3 mm Platform leveling ±0.1 mm	N/A
Material	Spool filament diameter 1.75 mm	Wood, acrylic, PCB, carbon fiber sheet, jade
Related power	400 W (max)	320 W

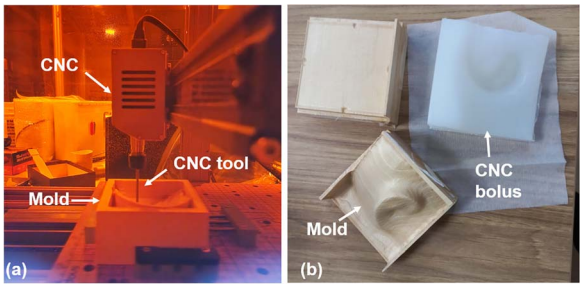

Fig. 5. Molds fabricated by CNC (a) and their resulting boluses using CNC mold (b).

Autodesk. The final toolpath files were prepared in g-code, the most widely used CNC programming language, which is used to instruct machines what to do. To minimize the difference from the 3D printing method, the layer setting was set to 0.15 mm. A single ball-end drill with a diameter of 3.175 mm was used to minimize human interference in the manufacturing process because Snapmaker 2.0 does not support auto tool change. The rest settings were prepared to optimize the toolpath and its speed appropriate to the material removal, which were a feed rate of 450 mm/min and 12,000 rpm for sculpting the wood stock.

The total manufacturing time of the mold cavities was 11 and 13 h for the ear and nose bolus, respectively, including the postprocessing and assembly of the mold cavity. In general, the manufacturing time was greatly reduced with CNC compared to 3DP. However, the lacking absolute experience with operating CNC machines in manufacturing mold resulted in requiring much more time in preparing the files compared to 3DP. The preparation time for 3DP files took ∼1.5 h, while for CNC files it took ∼8 h. This difference in the preparation time was expected to be reduced under identical levels of experience in operating both types of manufacturing devices. Overall, CNC manufacturing required less time compared to 3DP manufacturing. Pictures of the mold fabricating process and their resulting molds by CNC are shown in Fig. 5.

Bolus fabrication

When the molds were ready, the bolus was manufactured by filling the mold with platinum-catalyzed silicones and then waiting for hardening. This process took ∼4 h to be finished. Through several treatment cases and studies of the bolus material [12, 31], Ecoflex™ 0030 (Smooth On, Inc., Easton, PA, USA) [31–33] was selected to construct the patient-specific boluses using 3DP and CNC molds. Mass density of the bolus material was 1.105 g/cm^3, and its Hounsfield unit was set to 120 [31]. The resulting boluses were referred to as 3DP and CNC boluses in this report.

Evaluating method of the geometric property

Fabricated boluses were CT-scanned and imported to the Eclipse to make its RS structure. The RS files were then exported into the STL format for evaluation of their correspondence with the intended bolus structure. Consequently, there were three pairs (ear and nose) of STL structure files: one pair was the virtual bolus structures from the treatment plans, called original model files; two other pairs were from CT images of the 3DP and CNC boluses. In total, six STL files were paired to evaluate the resemblance between the planned and fabricated bolus structures. For the CT sacn, the bolus was positioned such that the surface meets the skin to be faced up, thus the flat face with studs was faced down. Due to the flexible nature of the bolus material, the curved surface which affects the air gap was considered significant for this evaluation. Hence, the structures were aligned based on surface points with the least deformation.

Once the structures were aligned, they were trimmed to only remain the significant faces. The trimming was conducted using the 'plane cut' feature of Meshmixer, such that each set of mesh files was of identical sizes. Those files were then imported to Meshlab (Visual Computing Lab, ISTI-CNR, Pisa, Italy) [34, 35], a program that can compare mesh (structure) files. A comparison of structure files was conducted following the procedure outlined by University of Pisa [36]. In Meshlab, pairs of STL files were imported to proceed with the Hausdorff distance calculation [37]. These calculations provided the maximum distances among the minimum distance between the two mesh files, representing quantified measures of the maximum geometrical deviance of the two structures. The minimum distances were in the order of 10^{-4} mm for all four comparisons and were considered to be negligible since they were smaller than the accuracy of the device used to scan and model the manufactured bolus, which was 1 mm.

Evaluating method of the dosimetric property

We repeated setting up the bolus on the phantom and measured the delivered dose three times independently to estimate the human setup error, although the treatment was prescribed to be conducted in a single

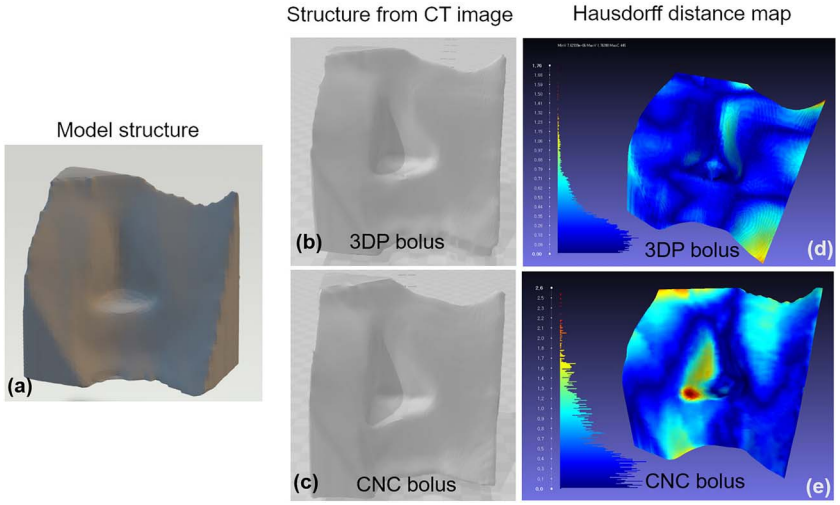

Fig. 6. Screenshot of Meshlab (Visual Computing Lab, ISTI-CNR, Pisa, Italy) comparing the (a) original nose bolus structure to the CT-scanned nose bolus manufactured by (b) 3DP mold and (c) CNC mode, depicting the Hausdorff distance in RGB color scheme for (d) 3DP and (e) CNC bolus.

session. As the material was opaque, the phantom with the bolus was aligned to the treatment room laser based on the studs on top surface of the bolus. To adhere the bolus to the rigid and sleek surface of the head phantom, taping was necessary for the bolus setup, which led to ease of deformation due to the flexibility of the bolus material. If the bolus deformation occurred through this process, the distance from the source to the bolus surface could be changed or the setup isocenter could be moved a few millimeters away from the beam center. With the 3DP and CNC boluses covering the lesion as determined in the plan, two points around the lesion were selected for the dose evaluation; comparing planned to measured doses and comparing the measured doses by using CNC versus by using 3DP boluses. Those points were marked on the picture of the head phantom in Fig. 1 and in the treatment plans (Figs 2 and 3). Delivered dose at each point was measured using MOSFET dosimeters (model TN-502RD-H). The dosimeters were connected to a mobile MOSFET reader (model TN-RD-16), where the measured doses were obtained in the mobile MOSFET software (v2.4). All of those MOSFET dosimeters and devices are products of Best Medical Canada (Ottawa, ON, Canada).

RESULTS

Geometric evaluation

Figures 6 and 7 show (a) the original model structure and CT-scanned image of resulting boluses made by (b) 3DP mold (c) and CNC mold. The calculated distances, between (b) and (a) and between (c) and (a), are then visualized through the Quality Mapper in the Meshlab as depicted in (d) and (e), respectively, in the figures. The maximum and mean values of the surface distances are summarized in Table 3. The Hausdorff distances were measured mostly submillimeter but with a few exceptions. These outliers arose from the area with a high gradient. While the mean distance was measured even <0.5 mm, the maximum Hausdorff distance was 2.6 mm for the CNC nose bolus and 1.63 mm for the 3DP ear bolus, respectively.

Dosimetric evaluation

Averaged values of the measured dose on the selected points and their standard deviations (SDs) were listed with the calculated dose by the TPS in Table 4. The difference between the measured and calculated doses ranged from 0.3 to 5.8%. The difference between the measured doses using either bolus, however, was measured to be less than 2.3%.

DISCUSSION

Geometric evaluation

An overhang in the 3D printing means a geometric feature that extends over the preprinted layer and thereby lacks direct support from layers below this feature. Therefore, it requires an extra support structure that subsequently needs postprocessing of the output mold. CNC was also challenged to fabricate the mold with the overhang. Adopting a smaller diameter of the CNC tool (as indicated in Fig. 5a) can overcome such limitations. However, in this study, we limited ourselves not to exchanging CNC tools to minimize manufacturing time. Despite the limit, the CNC output mold was comparable with the 3DP mold in the surface distance measurement. As the air gap under 5 mm was understood not to significantly affect the delivered dose [1, 38, 39], the geometric deviation analyzed in this study was not significantly accounted for as the source of dose difference uncertainty.

This limitation of CNC can be overcome by using a CNC machine that supports tool exchange, or that operates with more axis allowing the motion required in the machining of overhang features. However, these higher specifications of machines often require a much higher initial cost of acquiring the device and increased difficulty in operating the device. CNC machining is not constrained to layer height since it is subtractive manufacturing that removes molding material. In contrast to CNC, 3DP is constrained to layer height because it adheres to molding materials. The 3D printing by its nature needs to melt plastic to adhere layer by layer, limiting the improvement of its performance in terms of geometric resolution. Physical properties of the bolus

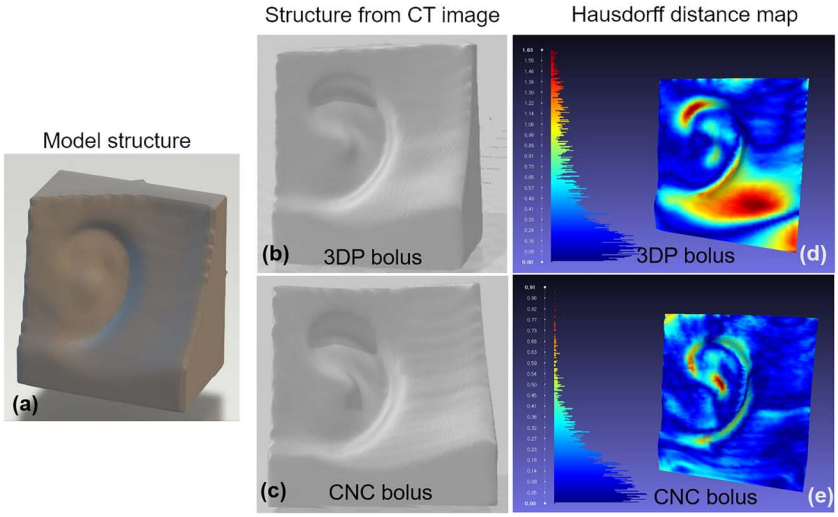

Fig. 7. Screenshot of Meshlab (Visual Computing Lab, ISTI-CNR, Pisa, Italy) comparing the (a) original ear bolus structure to the CT-scanned ear bolus manufactured by (b) 3DP mold and (c) CNC mode, depicting the Hausdorff distance in RGB color scheme for (d) 3DP and (e) CNC bolus.

Table 3. Maximum and mean Hausdorff distance (in mm) between the fabricated boluses and the original model structure

Distance	Nose		Ear	
	Maximum (mm)	Mean ± RMS (mm)	Maximum (mm)	Mean ± RMS (mm)
3DP bolus	1.76	0.25 ± 0.33	1.63	0.50 ± 0.64
CNC bolus	2.60	0.46 ± 0.59	0.91	0.20 ± 0.26

RMS = root-mean-square

Table 4. Summary of the calculated dose and averaged measured doses with their SD on the selected points near the lesions of ear and nose under the patient-specific bolus

Dose measurement	Nose		Ear	
Measurement point	A	B	A	B
Calculated dose (cGy)	1011	1007	1047	1014
Measurement with CNC bolus (cGy)	1050 ± 17	1020 ± 17	1050 ± 10	1033 ± 12
Relative difference (%)	3.86	1.29	0.29	1.87
Measurement with 3DP bolus (cGy)	1070 ± 10	1043 ± 15	1033 ± 6	1027 ± 6
Relative difference (%)	5.84	3.57	−1.34	1.28

material and more discussions including the air gap measurement of the patient-specific bolus fabricated by the mold-and-cast method can be found in the references [11, 31]. CNC machining showed comparable results and potential for performance improvement through a stable process. In terms of operators, 3D printing required much less training and experience compared to CNC machining because CNC has more room for operators to manage in the machining option.

Dosimetric evaluation

Although this difference can be clinically acceptable, here we contemplate the sources of uncertainty in measuring the delivered dose with MOSFET detectors. The uncertainty sources were divided into three categories: treatment setup, eMC accuracy in the TPS, and the MOSFET dosimeters.

Treatment setup uncertainty was estimated by repeating the dose measurement three times independently per bolus. Physical features of the patient-specific bolus material, opacity and flexibility, and the rigid and slick surface of the head phantom might cause uncertainty of the treatment reproducibility in a combination.

Although the eMC model describes dose distributions better than the conventional deterministic dose calculation algorithms [40, 41], it still gives a broad distribution in the dose difference between measurement and calculation, resulting in the dose calculation uncertainty. Sung *et al.* reported that the averaged dose difference between the

Table 5. Source of uncertainties for dosimetric evaluation

Sources of uncertainty	Details	Uncertainty (%)
Treatment setup	CNC Ear bolus	1.1
	3DP Ear bolus	0.6
	CNC Nose bolus	1.7
	3DP Nose bolus	1.5
eMC	Statistical uncertainty	2
MOSFET	Dosimeters for high dose irradiation [45–48]	5
	Creep-up effect [44]	8

eMC calculation and measurement was 1.52%, but the maximum dose difference went up to 6.09% using the same linear accelerator used in this study [42]. Carver *et al*. reported that the SD of the eMC dose difference was 2.38% for the less irregular surface (i.e. retromolar trigone region) with the 3D bolus, while it was increased to 3.35% for more irregular surface (i.e. the nose treatment with 3D bolus due to high gradient of the nose anatomy) [43]. The deviation between the measured and calculated dose used to be showing a larger SD when measuring the dose using bolus on the human phantom than the measurement in the ideal water due to the uncertainty coming from the heterogeneous structure of the phantom and irregular surface.

Concerning the MOSFETs, vendor-provided data sheets mention that the MOSFET dosimeters were operated with either standard (1 mV/cGy) or high sensitivity (3 mV/cGy) bias. Those bias selection brought different dose reproducibility uncertainty. The dose measurement in this report was made with the standard bias, which was expected to add more uncertainty. The fundamental dosimetric characteristics of the MOSFET dosimeters up to 630 cGy were investigated in detail in the study performed by Manigandan and his colleagues [44]. Interestingly, they reported another possible uncertainty from enhanced MOSFET reading caused by the 'creep-up effect'. When the readings were made continuously, a maximum deviation of up to 8% was found. This effect was not realized at the time of dose measurement with phantom, but it should be considered a source of uncertainty too. Dose measurement uncertainty of MOSFETs above 630 cGy was evaluated for intraoperative radiation therapy, which uses a dose of up to 23 Gy. Consorti *et al*. [45] reported that their *in vivo* results were in agreement with the predicted dose values within 5%, and other studies [46–48] estimated the uncertainty of the MOSFET dosimeters in the range of 1.5–5%.

Investigated sources of dose measurement uncertainty are listed in Table 5.

CONCLUSION

This study focuses on the molding modality to manufacture patient-specific bolus spending less time. Comparing the boluses fabricated by the CNC and 3DP molds, we have observed no significant differences in both geometric and dosimetric evaluations. The 3DP and CNC molding methods are complementary, thus allowing one to choose the preferred molding method based on occasion demands. However, the CNC molding method benefits from the time-saving and its stable process of fabrication, and this is effective for the keloid treatment.

CONFLICT OF INTEREST

The authors have no relevant conflict of interest to disclose.

FUNDING

This work was supported by a grant from Seoul National University Hospital [420202190, 420220290].

DATA AVAILABILITY

The authors confirm that the data supporting the findings of this study are available within the article.

REFERENCES

1. Butson M-J, Cheung T, Yu P *et al.* Effects on skin dose from unwanted air gaps under bolus in photon beam radiotherapy. *Radiat Meas* 2000;32:201–4.
2. Khan Y, Villarreal-Barajas J-E, Udowicz M *et al.* Clinical and dosimetric implications of air gaps between bolus and skin surface during radiation therapy. *J Cancer Ther* 2013;4:1251–5.
3. Wang K-M, Rickards A-J, Bingham T *et al.* Technical note: evaluation of a silicone-based custom bolus for radiation therapy of a superficial pelvic tumor. *J Appl Clin Med Phys* 2022;23:e13538.
4. Lobo D, Banerjee S, Srinivas C *et al.* Influence of air gap under bolus in the dosimetry of a clinical 6 MV photon beam. *J Med Phys* 2020;45:175–81.
5. Aldawood F-K, Chang S-X, Desai S. Design and manufacture of a high precision personalized electron bolus device for radiation therapy. *Med Devices Sens* 2020;3:e10077.
6. Wang X, Wang X, Xiang Z *et al.* The clinical application of 3D-printed boluses in superficial tumor radiotherapy. *Front Oncol* 2021;11:698773.
7. Burleson S, Baker J, Hsia A-T *et al.* Use of 3D printers to create a patient-specific 3D bolus for external beam therapy. *J Appl Clin Med Phys* 2015;16:166–78.
8. Song J-H, Jung J-Y, Park H-W *et al.* Dosimetric comparison of three different treatment modalities for total scalp irradiation: the conventional lateral photon-electron technique, helical tomotherapy, and volumetric-modulated arc therapy. *J Radiat Res* 2015;56:717–26.
9. Park S-Y, Choi C-H, Park J-M *et al.* A patient-specific polylactic acid bolus made by a 3D printer for breast cancer radiation therapy. *PLoS One* 2016;11:e0168063.
10. Kim S-W, Kwak J, Cho B *et al.* Clinical implementation of 3D printing in the construction of patient specific bolus for photon beam radiotherapy for mycosis fungoides. *Prog Med Phys* 2017;28:33–8.

11. An H-J, Kim M-S, Kim J *et al.* Geometric evaluation of patient-specific 3D bolus from 3D printed Mold and casting method for radiation therapy. *Prog Med Phys* 2019;30:32–8.
12. Park J-M, Son J, An H-J *et al.* Bio-compatible patient-specific elastic bolus forclinical implementation. *Phys Med Biol* 2019;64:105006.
13. Chatchumnan N, Kingkaew S, Aumnate C *et al.* Development and dosimetric verification of 3D customized bolus in head and neck radiotherapy. *J Radiat Res* 2022;63:428–34.
14. Nematollahi B, Xia M, Sanjayan J. Post-processing methods to improve strength of particle-bed 3D printed geopolymer for digital construction applications. *Front Mater* 2019;6:00160.
15. Karakurt I, Lin L. 3D printing technologies: techniques, materials, and post-processing. *Curr Opin Chem Eng* 2020;28:134–43.
16. Chen Y-F, Wang Y-H, Tsai J-C. Enhancement of surface reflectivity of fused deposition modeling parts by post-processing. *Opt Commun* 2019;430:479–85.
17. Low D-A, Starkschall G, Sherman N-E *et al.* Computer-aided design and fabrication of an electron bolus for treatment of the paraspinal muscles. *Int J Radiation Oncology Biol Phys* 1995; 33:1127–38.
18. Kim I-S, McLean W. Computing the Hausdorff distance between two sets of parametric curves. *Commun Korean Math Soc* 2013;28:833–50.
19. Birsan T, Tiba D. One hundred years since the introduction of the set distance by dimitrie pompeiu. In: Ceragioli F, Dontchev A, Furuta H, Marti K, Pandolfi L (Eds). *IFIP International Federation for Information Processing*, Turin, Italy. Boston, MA, USA: Springer, 2005, Vol. 199, pp. 35–39.
20. Berman B, Bieley HC. Adjunct therapies to surgical management of keloids. *Dermatol Surg* 1996;22:126–30.
21. Lee S-Y, Park J. Postoperative electron beam radiotherapy for keloids: treatment outcome and factors associated with occurrence and recurrence. *Ann Dermatol* 2015;27:53–8.
22. Guix B, Henríquez I, Andrés A *et al.* Treatment of keloids by high-dose-rate brachytherapy: a seven-year study. *Int J Radiat Oncol Biol Phys* 2001;50:167–72.
23. Borok T-L, Bray M, Sinclair I *et al.* Role of ionizing irradiation for 393 keloids. *Int J Radiat Oncol Biol Phys* 1988;15:865–70.
24. Kovalic J-J, Perez C-A. Radiation therapy following keloidectomy: a 20-year experience Jeffrey. *Int J Radiat Oncol Biol Phys* 1989;17:77–80.
25. Escarmant P, Zimmermann S, Amar A *et al.* The treatment of 783 keloid scars by iridium 192 interstitial irradiation after surgical excision. *Int J Radiat Oncol Biol Phys* 1993;26:245–51.
26. Ogawa R, Miyashita T, Hyakusoku H *et al.* Postoperative radiation protocol for keloids and hypertrophic scars. *Ann Plast Surg* 2007;59:688–91.
27. Hwang N-H, Nam K-L, Chae J-H *et al.* The efficacy of CT-based conformal electron beam radiation therapy after keloid excision. *Dermatol Surg* 2022;48:435–40.
28. Song C, Wu H, Chang H *et al.* Adjuvant single-fraction radiotherapy is safe and effective for intractable keloids. *J Radiat Res* 2014;55:912–6.
29. Vyavahare S, Teraiya S, Panghal D *et al.* Fused deposition modeling: a review. *Rapid Prototyp J* 2020;26:176–201.
30. Jo K-H, Jeong Y-S, Lee J-H *et al.* A study of post-processing methods for improving the tightness of a part fabricated by fused deposition modeling. *Int J Precis Eng Manuf* 2016;17:1541–6.
31. Son J, Jung S, Park J-M *et al.* Evaluation of platinum-catalyzed silicons for fabrication of biocompatible patient-specific elastic bolus. Preprint. https://doi.org/10.21203/rs.3.rs-48004/v1.
32. Eom S, Lim S. Stretchable complementary split ring resonator (CSRR)-based radio frequency (RF) sensor for strain direction and level detection. *Sensors* 2016;16:s16101667.
33. Mantzavinou A. Sustained-release implants for intraperitoneal cisplatin delivery. *Doctoral Dissertation*. Messachusetts Institute of Technology 2018.
34. Cignoni P, Callieri M, Corsini M *et al.* MeshLab: an open-source mesh processing tool. In: Scarano V, De Chiara R, Erra U (Eds). *Eurographics Italian Chapter Conference*, Salerno, Italy. Organized online: The Eurographics Association, 2008, pp. 129–136.
35. Ranzuglia G, Callieri M, Dellepiane M *et al.* MeshLab as a complete tool for the integration of photos and color with high resolution 3D geometry data. In: *CAA 2012 Conference Proceedings*, Southampton, UK. Amsterdam, The Netherlands: Amsterdam University Press, 2013, pp. 406–416.
36. Dellepiane M, Scopigno R. Teaching 3d acquisition for cultural heritage: a theory and practice approach. In: *Proceedings of Eurographics Conference 2012-Education Papers*, Cagliari, Sardinia, Italy. Organized online: The Eurographics Association, 2012, pp. 25–32.
37. Cignoni P, Roccini C, Scopigno R. Metro: measuring error on simplified surfaces. *Comput Graph Forum* 1998;17:167–74.
38. Dyer B-A, Campos D-D, Hernandez D-D *et al.* Characterization and clinical validation of patient-specific three-dimensional printed tissue-equivalent bolus for radiotherapy of head and neck malignancies involving skin. *Phys Med* 2020;77: 138–45.
39. Shaw E, Kline R, Gillin M *et al.* Radiation therapy oncology group: radiosurgery quality assurance guidelines. *Int J Radiat Oncol Biol Phys* 1993;27:1231–9.
40. Ma C-M-C, Chetty I-J, Deng J *et al.* Beam modeling and beam model commissioning for Monte Carlo dose calculation-based radiation therapy treatment planning: report of AAPM task group 157. *Med Phys* 2020;47:e1–18.
41. Wanklyn M-D, Kidane G, Crees L. Verification measurements of an eMC algorithm using a 2D ion chamber array. *J Appl Clin Med Phys* 2016;17:320–8.
42. Sung J, Jin H, Kim J *et al.* Improvement of calculation accuracy in the electron Monte Carlo algorithm with optional air profile measurements. *Prog Med Phys* 2020;31:163–71.
43. Carver R-L, Sprunger C-P, Hogstrom K-R *et al.* Evaluation of the eclipse eMC algorithm for bolus electron conformal therapy using a standard verification dataset. *J Appl Clin Med Phys* 2016;17:52–60.
44. Manigandan D, Bharanidharan G, Aruna P *et al.* Dosimetric characteristics of a MOSFET dosimeter for clinical electron beams. *Phys Med* 2009;25:141–7.
45. Consorti R, Petrucci A, Fortunato F *et al.* In vivo dosimetry with MOSFETs: dosimetric characterization and first clinical results

in intraoperative radiotherapy. *Int J Radiation Oncology Biol Phys* 2005;63:952–60.

46. Petoukhova A, Rüssel I, Nijst-Brouwers J *et al.* In vivo dosimetry with MOSFETs and GAFCHROMIC films during electron IORT for accelerated partial breast irradiation. *Phys Med* 2017;44:26–33.
47. Hensley F-W. Present state and issues in IORT physics. *Radiat Oncol* 2017;12:37.
48. Dai G, Xu X, Wu X *et al.* Application of 3D-print silica bolus for nasal NK/T-cell lymphoma radiation therapy. *J Radiat Res* 2020;61:920–8.